Journal of Physics and Chemistry of Solids 74 (2013) 558–564

Contents lists available at SciVerse ScienceDirect

Journal of Physics and Chemistry of Solids

journal homepage: www.elsevier.com/locate/jpcs

Hydrogen adsorption study on mixed oxides using the density functional theory

M. Abdus Salam*, Suriati Sufian, Ye Lwin

Chemical Engineering Department, Universiti Teknologi PETRONAS, Bandar Seri Iskandar, 31750 Tronoh, Perak, Malaysia

ARTICLE INFO

Article history:
Received 10 July 2012
Received in revised form
9 November 2012
Accepted 4 December 2012
Available online 14 December 2012

Keywords:
A. Reduced mixed oxide
B. Chemical synthesis
C. Density functional theory
D. Favorable thermodynamics
D. Phase equilibria

ABSTRACT

Density functional theory (DFT) calculation has been performed successfully to explore hydrogen adsorption capacity of reduced cobalt and nickel containing mixed oxides. Hydrogen adsorption behaviors of mixed oxides have been discussed via few reactivity descriptors at the M05-2X/6-311+G (d, p) level of theory. Calculated various types of energetic, reaction enthalpies and electrophilicities of cobalt and nickel clusters which are at minimum energy on potential energy surface concerned with the hydrogen adsorption phenomena attributed that reduced nickel and cobalt mixed oxides is an effective hydrogen storage material. The dynamic adsorption method as an experimental investigation has been carried out to find the performance or adsorption trend of mixed oxides. The trends of computational and experimental results are consistent in regards to hydrogen adsorption. Thermochemistry analysis predicted the phenomena are chemisorption dominant. Reduced cobalt and nickel mixed oxides are believed to be promising hydrogen storage materials where 13 wt% hydrogen capacities are obtained. Thus the density functional theory is an efficient tool to explore this hydrogen storage capacity.

1. Introduction

Hydrogen is one the green energy carrier and a source of future energy due to its renewal ability, non-polluting nature, and high energy density (142 MJ/kg) per unit mass; moreover, it can be derived from various domestic resources.

Mixed oxides have remarkably important features in forming of highly dispersed metallic particles upon reduction. The surface of the reduced form of the mixed oxides is more reactive than the oxide form with gases (ambient or higher temperature) and can form possible yields. The hydrogen adsorption phenomena on oxides such as ZnO, TiO_2, ZrO_2 and mixed oxides $CeM_{0.5}Ni_xO_y$ were investigated through experimentations as well as theoretical approaches [1–5]. The $CeM_{0.5}Ni_xO_y$ mixed oxide showed a 10 wt% hydrogen adsorption capacity but is not sufficient enough economically due to the expensive novel Cerium metal. Adsorption on the cobalt and nickel surfaces has been carried out with a thin film of a supported catalyst and nickel (or cobalt)/graphite composites which showed the capacity 2.8 wt% [6–8]. Adsorption of hydrogen on metal mixed oxides such as nickel and cobalt oxides have not been studied extensively yet. There is still a lack of theoretical and experimental adsorption knowledge on mixed oxides. An adsorption study on bi metallic/tri-metallic materials is complicated. Nickel has very low activation energy for hydrogen adsorption whereas cobalt has higher activation energy for hydrogen chemisorption and has a kinetic barrier at lower temperature [9]. A certain amount of energy is needed to trap hydrogen to every system or cluster. Physisorption is not fully able to meet the hydrogen storage goal. Therefore, efforts have been focused on porous materials and chemisorption along with physisorption.

Reversible hydrogen storage systems adsorb hydrogen with the energy between physisorption and chemisorption where the hydrogen is stored predominantly in a molecular form [10]. Those having lower formation energy require special conditions (high pressure or temperature) to adsorb hydrogen. Medium stable clusters are suitable enough to release or desorb hydrogen by less amount of energy (heat). Magnesium and magnesium-nickel hydrides contain a relatively high fraction of hydrogen by weight, but need to be heated to at least 250 or 300 °C in order to release the hydrogen [11]. The maximum hydrogen atoms can bind with the nickel/cobalt to their octahedral site to form hydride. Moreover, there are possibilities for binding hydrogen between a hydride legend and hydrogen molecules or atoms [12]. For transitional metals, d orbital fills up with electrons and is promoted to a higher energy orbital due to the rising atomic number. Hydrogen not only shares electron with the metal during formation of hydride but also lowers the states bottom of the d band. So the capturing effect is balanced by lowering the orbital energies along with increasing the nuclear charges.

* Corresponding author. Tel.: +60 192912198; fax: +60 75-3656176.
E-mail address: salam.bcsir@gmail.com (M. Abdu Salam).

0022-3697/$ - see front matter © 2012 Elsevier Ltd. All rights reserved.
http://dx.doi.org/10.1016/j.jpcs.2012.12.004

To deepen the understanding of the hydrogen adsorption mechanism on reduced mixed oxides, a detailed and clear insight is needed which are constituted with many physiochemical parameters and it is difficult to get all this information from experiments. A theoretical study or DFT study can be an alternative tool in order to compute the required physiochemical parameters or descriptors due to having many functional which describe the energetic interaction of an electron with other electrons, kinetics and thermodynamics. Hydrogen adsorption on the ZnO nanotube [13], $Mg_{0.75}Ti_{0.25}$ alloy [14], Alanates [15(a,b)], metal-organic frameworks (MOF's) [16–18] and activated carbon etc. [19,20(a,b,c)] as well as metal hydrides (MgH_2, AlH_3) [21(a,b)] and metal borohydrides (LiBH4, NaBH4) [22] were carried out using the DFT method, but none of them meets the department of energy (DOE, U.S.A) goals for reversible hydrogen storage materials. To date, more attention has been focused to the hydrogen adsorption on mixed oxides. The DFT method can be applied to identify an economic adsorbent and to understand the H_2 adsorption mechanism on mixed oxides by considering related descriptors. Electronic structure principles such as the maximum hardness (MHP) [23], minimum polarizability (MPP) [24] and minimum electrophilicity (MEP) [25] principles are capable in determining the thermodynamic stability of molecular system. Thermodynamic descriptors like reaction enthalpy, gibb's free energy, reaction rates, electrophilicity and different types of energy like interaction, adsorption, formation and desorption energy can predict the adsorption feasibility of a material [26]. An investigation on homogenous reduced mixed oxides has surprisingly shown good adsorption capacity.

The objectives of this study are to predict hydrogen adsorption capacity of mixed oxides and the stability of hydrogen adsorbed cluster and to see whether the incorporation of a gradual number of hydrogen is thermodynamically and kinetically favorable.

2. Methods

2.1. Experimental method

Ni-Co-Cr Hydrotalcite with different molar ratios has been synthesized using coprecipitation method [27]. Metal nitrate precursors and Na_2CO_3 as the precipitating agent were used to prepare the adsorbents. The resulting samples were calcined in a furnace at 500 °C for 2 h to obtain mixed oxides. The calcined materials or mixed oxides are designated by NCCMO-xyz where NCCMO stands for Nickel–Cobalt–Chromium mixed oxide, xyz stands for the molar ratios of Ni:Co:Cr.

The mixed oxides were analyzed by powder X-ray diffraction (XRD) technique using a Bruker D8 advanced diffractometer with Cu-K_α radiation ($\lambda=0.154$ nm). Diffraction patterns were recorded in the range of $2\theta=3$–80° with a step size of 0.04° and a counting time per step of 10 s. Mixed oxides reductions have been performed by temperature-programmed reduction (TPR) technique using a Thermo Finnigan TPD/R/O 1100 instrument. A 20–25 mg sample was reduced by a 10% H_2-in-Ar flowing at 20 ml/min, with heating rate of 10 °C/min up to 800 °C. It was than cooled down without gas flow to room temperature. Later, hydrogen gas (10% H_2-in-Ar) was exposed with similar experimental condition and heated from room temperature to 500 °C for adsorption study.

2.2. Computational method

Geometries optimization of the cluster and calculation of its electronic energy, vibrational frequencies and related descriptors for the hydrogen captured system had been carried out using the hybrid meta exchange-correlation functional, M05-2X [28] in combination with the 6-311+G(d, p) basis set [29]. To obtain a stable wave function and to recover a larger fraction of the exchange-correlation energy, multiple function; 6-311+G(d, p) had been used. The M05-2X functional was more precise for calculation of the thermochemistry and non-covalent interaction especially weak interaction, hydrogen bonding, and interaction energies of nucleobases [28]. Geometry optimization of the clusters and its frequency calculation (using the functional, M05-2X) was carried out to ensure the minima on potential energy surface (PES) and generated acceptable values of global descriptors which were consistent with the experimental results. All calculations had been performed by using the GAUSSIAN 09W program package [30]. The second derivative calculation had been done at the optimized geometries to check the minima on the potential energy surface (real frequencies). Geometries of the optimized N-electron systems or clusters at the M05-2X/6-311+G(d, p) level of the theory had been used to determine the energies of the $N\pm1$ electron system by single point energy calculations. $IP=E(N\pm1)-E(N)$ and $EA=E(N)-E(N\pm1)$ values had been calculated using DFT energy calculations from the bottom of the potential well of the neutral. Electronegativity [31(a,b)], hardness [32(a,b,c)] and electrophilicity [33] were calculated by the generally used finite approximation; $\chi=IP+EA/2$ and $\eta=IP-EA$ and $\omega=\chi^2/2\eta$, respectively. Interaction energy (ΔE_i) per hydrogen molecule [34], adsorption energy (ΔE_{ads}), average desorption energy (ΔE_{DE}) per hydrogen atom [34], reaction enthalpies (ΔH_r) and Gibb's energies (ΔG_r) and electrophilicities ($\Delta\omega$) were calculated as the difference between the products and reactants according to the equation below [35]. The following expressions have been used to calculate the above descriptors;

Interaction energy of per hydrogen molecule to cluster:

$$\Delta E_i=(1/n)[E_{M(H_2)_n}-(E_M+nE_{H_2})];$$

where, n is the number of molecular hydrogen. E_M and E_{H_2} is the electronic energy of reduced metal and hydrogen molecule, $E_{M(H_2)_n}$ is the total energy of n number of adsorbed hydrogen.

Total hydrogen adsorption energy of the system:

$$\Delta E_{ads}=[E_M+nE_{E_2}]-E_{M(H_2)_n}$$

Desorption energy of per hydrogen atom:

$$\Delta E_{DE}=E_H+(1/2)[E_{SH_{n-2}}-E_{SH_n}];$$

where, n=number of hydrogen atoms and S is the hydrogen trapped system, $E_{SH_{n-2}}$ and E_{SH_n}=total energy of $(n-2)$ and n number of hydrogen adsorbed system, respectively.

Thermochemical parameters such as reaction enthalpy, Gibbs energy and formation energy calculation have been performed using following expression [35];

$$\Delta H_r(298.15\ \text{K})=\sum(\text{z.epsiv};_0+H_{corr})_{product}-\sum(\text{z.epsiv};_0+H_{corr})_{reactant}$$

$$\Delta G_r(298.15\ \text{K})=\sum(\text{z.epsiv};_0+G_{corr})_{product}-\sum(\text{z.epsiv};_0+G_{corr})_{reactant}$$

$$\Delta H_f(M,298.15\ \text{K})=\sum x\Delta H_f(x,298.15\ \text{K})-\sum D_0(C)$$

$\sum D_0(C)$ is the atomization energy of the clusters. Gaussian 09 'keywords' corresponding to temperature and pressure have been used to check the variation of the temperature–pressure dependent descriptors. The vibrational spectra of hydrogen trapped cluster have been investigated and characterized by a strong infrared (IR) active band.

3. Results and discussion

3.1. Experimental adsorption results on mixed oxides

Hydrotalcite decomposition can be performed following a few steps such as dehydration, dehydroxylation and the decomposition

of anions after that the final product is mixed oxides. At an intermediate calcination temperature it turns to the amorphous phase ($M^{II}_{(1-x)}M^{III}_{x}O_{1+x/2}$) [36] and again convert into the crystalline phase as equation below. X-ray diffraction spectrums of mixed oxides are shown in Fig. 1.

$$[M^{II}_{(1-x)}M^{III}_{x}(OH)_2](A^{n-})_{x/n} \times mH_2O \rightarrow [M^{II}_{(1-x)}M^{III}_{x}(OH)_2]^{x+}\ (A^{n-})_{x/n} \rightarrow$$

$$[M^{II}_{(1-x)}M^{III}_{x}O]^{x+}\ (A^{n-})_{x/n} \rightarrow M^{II}_{(1-x)}M^{III}_{x}O_{1+x/2}\ \rightarrow M^{II}O + M^{II}\ M^{III}_{2}O_4.$$

Converted mixed oxides such as ($M^{II}O$); NiO [JCPDS 01-1239(D)], CoO [JCPDS 09-0402(D)], Co_3O_4 [JCPDS 42-1467] and spinels $\left(M^{II}\ M^{III}_{2}O_4\right)$; $NiCr_2O_4$ [JCPDS 23-1272(N)], $CoCr_2O_4$ [JCPDS 24-0326 (N)] and $NiCo_2O_4$ [JCPDS 02-1074 (N)] can be assigned from the XRD spectrum (Fig. 1) of mixed oxides with different molar ratios. The situation of overlapping is also observed between NiO and some of the spinels. The decomposed phases of the Co_2O_3-like spinel and CoO or NiO are irreversible [37].

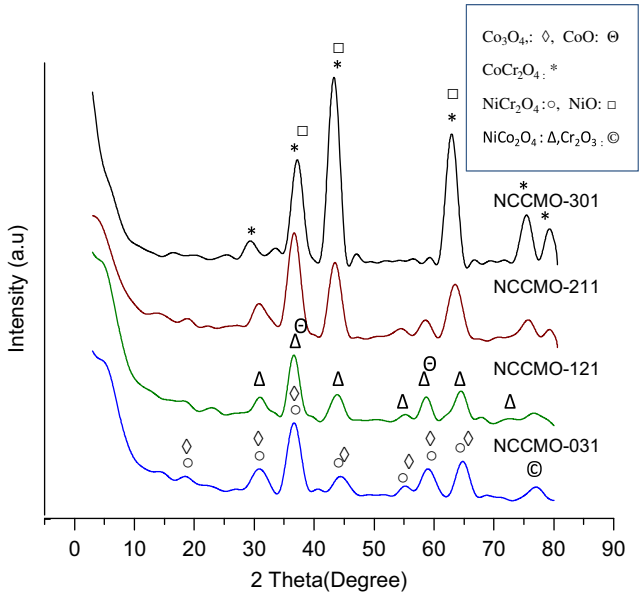

Fig. 1. XRD analysis for mixed oxides formations.

The results of the temperature programmed reduction of the mixed oxides are shown in Fig. 2. Two reduction peaks for NCCMO-031 are observed at 402 °C and 720 °C with respective broad shoulders. The first reduction peak with its broad shoulder represents successive reduction of Co^{3+} and Co^{2+} from the Co_3O_4 spinel: $Co_3O_4 \rightarrow CoO \rightarrow Co^0$ [38,39]. The second peak and its shoulder represent the parallel and series reduction of Co^{3+} and Co^{2+} from Co–Cr–O spinels: $Co_2CrO_4 \rightarrow CoCrO_3$ and $CoCr_2O_4 \rightarrow Co^0$. The TPR profile of NCCMO-301 indicates a peak at 495 °C which is due to the reduction of Ni from the free NiO phase. This peak occupied a bigger area as compared to other peaks, due to the overlapping with the reduction of the $NiCr_2O_4$ spinel.

Ternary mixed oxides, NCCMO-121 and NCCMO-211, shows different reduction patterns from those of binary oxides. The mixed oxides, NCCMO-121, i.e., Co rich ternary sample, the cobalt oxides and nickel oxides reduced to cobalt and nickel at 402 °C whereas the Ni rich ternary sample, (NCCMO-211) both oxides reduced to nickel and cobalt at 380 °C; they are influenced by each other. The solder-like peak at the 540–700 °C temperature range correspond to the reduction of $CoCr_2O_4$, $NiCr_2O_4$ and $NiCo_2O_4$ to their respective oxide and to the metal phase with the peaks overlapping. The reduction of the spinel phases of nickel and cobalt shows little deviation due to the effect of the supported metal chromium. $CoCr_2O_4$ and $NiCr_2O_4$ might not be reduced completely at temperature range of 25–800 °C since chromium is a support element of the investigated material.

H_2 adsorption on mixed oxides through a dynamic method is shown in Fig. 2(b). Nickel rich reduced oxides leads to a hydrogen adsorption below 100 °C and this is very significant adsorption for a reversible system. Cobalt rich reduced oxides also show a similar trend but not as dominant as nickel. Nickel rich reduced oxides adsorbed a major amount of hydrogen at 180 °C. But cobalt rich

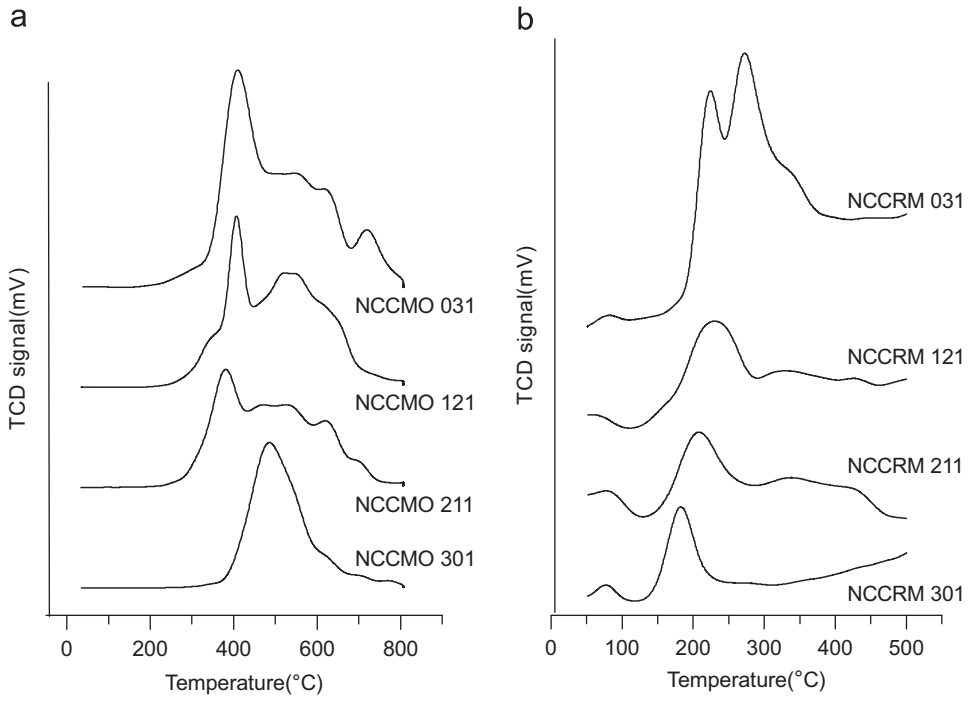

Fig. 2. (a) Reduction of mixed oxides (TPR). (b) H_2 adsorption by reduced oxides.

reduced oxides adsorbed H_2 at 225 and 270 °C and showed a steady trend at the 380–500 °C temperature range. Reduced nickel and cobalt mixed oxides (NCCRM-121 and NCCRM-211; NCCRM stands for NCC reduced mixed oxides) show almost a similar trend of hydrogen adsorption where the reduced nickel reached to a steady state earlier than the reduced cobalt. The reduced oxides of NCCRM-121 and NCCRM-211 obtained maximum adsorption at 230 and 210 °C and saturated at 290 and 270 °C, respectively. Present study reveals that the adsorption trend is chemisorption dominant. It is worth it to report that the TCD signal cannot be stabilized at lower temperatures which might be a reason for the absence of TCD signal (signal not shown at low temperature region). The adsorption behavior of nickel and cobalt with individual support shows its capacity where nickel could accelerate the adsorption rate that is shown in Fig. 2b. We avoid the chromium effect on the adsorption because of its contribution as a support element in synthesized material.

3.2. Theoretical study of hydrogen adsorption through density functional theory

The investigations have been carried out on the possible hydrogen adsorbed nickel and cobalt clusters are shown in Fig. 3. (Optimized cobalt clusters) Some conceptual density functional based global reactivity descriptors have been studied below to justify the possibility of hydrogen adsorption on reduced metals.

The interaction energy between reduced nickel or Cobalt oxide surface and the hydrogen molecules (gradually captured number of H_2) are reported in Table 1. The increasing trend of the interaction energies is observed between per hydrogen molecule and the reduced nickel or cobalt oxides with increase number of hydrogen molecules. The increasing trend of interaction energy and the adsorption energy value of the clusters upon gradual captured number of hydrogen indicate the favorable hydrogen adsorption on reduced oxides and that are in chemisorption range (>12 kcal/mol). By comparing the calculated data, (Table 1) the molecular interaction can be classified as electrostatic (≥ 20 kcal/mol) and strong hydrogen bonding type interaction (≤ 20–40 kcal/mol). On the contrary, decreasing trend is an indication of unfavorable adsorption for higher amount of hydrogen. In this sense, with an increasing loading number of hydrogen molecules, cobalt has higher hydrogen capacity than that of nickel. The average desorption energies [Table 1] of the investigated systems (Nickel or Cobalt cluster) attributed that desorption may occur at higher temperature for the minimum adsorbed hydrogen and maximum adsorbed hydrogen desorb at low temperatures. Also this desorption energy depend on the metal, temperature and nature of the adsorbents. Most of the cluster's formation energy is negative and indicate that the hydrogen adsorption phenomena are exothermic. Both clusters formed through chemisorption of hydrogen since formation energies are small and need special pressure or temperature. In a mixed oxides, M–O–M′ system [for example: $Co_2CrO_4 = Co^{3+}(Cr^{3+}Co^{3+})O_4^-$ or $Cr^{3+}(Cr^{3+}Co^{3+})O_4^-$], the binding energy of the metals are generally altered [40]. Any of them (Cr^{3+} or Co^{3+}/Co^{2+}) might be more ionic and produce an electric field. So, the polarized hydrogen molecules by those ions can then bind to it in a quasi-molecular form [41] which is intermediate between physisorption and chemisorption and can be desorbed at a higher temperature. Hydrogen has a low barrier of adsorption on both reduced cobalt and nickel surface. Reduced mixed oxides surface accelerate the adsorption of molecular hydrogen by creating less barrier and dipole difference between the reduced mixed oxides. Nickel catalyzes hydrogen adsorption onto cobalt by enhancing the dissociation of adsorbed hydrogen molecules.

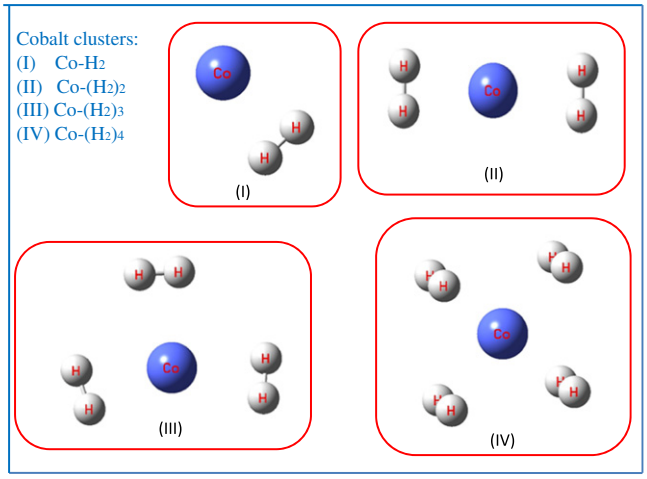

Fig. 3. Optimized structure of Co-(H_2)n (where n=1,2…4) clusters at M05-2X /6-311+G(d, p) level of theory.

Table 1
Adsorption and desorption related energy descriptors.

Cluster	ΔE_i (kcal/mol)	ΔE_{ads}, (kcal/mol)	ΔE_{des}, kcal/mol	ΔH_f (kcal/mol)	$\Delta\omega$ (kcal/mol)
Ni-(H_2)	−30.80	30.80	68.95	−137.88	102.84
Ni-(H_2)$_2$	−27.25	54.49	65.38	−249.42	64.08
Ni-(H_2)$_3$	−23.63	70.87	61.73	−362.87	31.81
Ni-(H_2)$_4$	−14.03	56.90	46.15	−484.38	3.23
Co-(H_2)	−22.49	22.49	64.78	−120.87	−16.37
Co-(H_2)$_2$	−45.97	91.96	88.27	−287.36	−37.81
Co-(H_2)$_3$	−34.56	103.71	59.42	−396.72	−63.16
Co-(H_2)$_4$	−20.61	82.46	42.90	−468.59	−83.91

Note: Interaction energy(ΔE_i), adsorption energy (ΔE_{ads}), desorption energy (ΔE_{des}), heat of formation (ΔH_f), reaction electrophilicity ($\Delta\omega$).

Table 2
Adsorption thermodynamics and kinetics descriptors.

Cluster	At temp. 298 K		At temp. 773 K		Rate of adsorption (at 773 K), (s^{-1})
	ΔH_r (kcal/mol)	ΔG_r (kcal/mol)	ΔH_r (kcal/mol)	ΔG_r (kcal/mol)	
Ni-(H_2)	−30.55	−25.37	−31.64	−32.98	3.4×10^{22}
Ni-(H_2)$_2$	−50.71	−38.14	−51.82	−50.39	2.8×10^{27}
Ni-(H_2)$_3$	−64.06	−44.55	−67.02	−59.49	1.0×10^{30}
Ni-(H_2)$_4$	−48.14	−27.47	−48.60	−58.68	6.2×10^{29}
Co-(H_2)	−19.93	−16.38	−22.33	−23.26	6.0×10^{19}
Co-(H_2)$_2$	−88.59	−76.84	−89.17	−89.62	3.5×10^{38}
Co-(H_2)$_3$	−98.54	−79.85	−98.51	−98.36	8.4×10^{55}
Co-(H_2)$_4$	−72.06	−43.20	−73.10	−61.17	5.9×10^{39}

Reaction enthalpy (ΔH_r), Gibb's free energy (ΔG_r) and rate of adsorption at 773 K.

The thermodynamic descriptors toward the hydrogen adsorption capacity of mixed oxides such as Gibbs free energies (ΔG_r) and enthalpy change (ΔH_r) were calculated to predict the feasibility of hydrogen adsorption on reduced nickel and Cobalt surface. The thermodynamic and kinetic data are calculated based on global minimum energy on potential energy surface (PES). The negative values of Gibb's free energies (ΔG_r) shown in Table 2, confirm the feasibility of the adsorption phenomenon at room temperature (298.15 K) and imply the spontaneous nature of hydrogen adsorption on reduced nickel and cobalt oxides surface [34]. At a higher temperature (773 K) the Gibb's energies are also negative and higher (average value) than that of 298.15 K values. Nickel and cobalt clusters showed increasing trend of reaction enthalpies and Gibb's energies (refer to Table 2). It was reported that the increasing trend is more favorable for chemisorption (enthalpy range 10–48 kcal/mol) [26]. By using Ni and Co clusters, the negative values of reaction enthalpies (ΔH_r) for hydrogen adsorption are estimated which reflect to the trapping of H_2 is exothermic. This phenomenon also confirms the possibility of physical adsorption (enthalpy limit 5–10 kcal/mol) due to the increase in temperature of the system. System entropy is decreasing upon captured increasing number of H_2 on the reduced surface due to the decrease of freedom of movement of hydrogen. At higher temperature (773 K) system show slow hydrogen adsorption kinetics that are in chemisorption level. The decreasing trend of reaction electrophilicity values are shown in Table 1 with an increasing number of hydrogen binding. This kind of trend attributed that the hydrogen trapping on reduced oxides is favorable [26].

Total electronic energy and thermodynamical stability descriptors such as the hardness, electronegatvity and electrophilicity of hydrogenated clusters are calculated and shown in Table 3. There is a gradual increase in the total electronic energy upon increasing number of captured hydrogen which also attributes the bonding nature of molecular hydrogen on reduced mixed oxides. The chemical potential (negative value of electronegativity) measures the escaping tendency of the electrons from the equilibrium state of the cluster member or system whereas the chemical hardness depict the strength of a cluster to charge transfer. According to the maximum hardness principle (MHP) and the minimum electrophilicity principle (MEP); a higher hardness value and lower electrophilicity value indicate the cluster most stable. According to the trend of the descriptors (Table 3) the cluster; Co-$(H_2)_4$ and Ni-$(H_2)_4$ are most stable than others. It was reported that hydrogen adsorption on 4d and 5d transitional metal (Platinum and palladium) clusters showed strong IR peaks at 1000–1500 cm^{-1} region associated with hydrogen bound to multiple metal atoms [42,43]. Cobalt and nickel clusters IR spectrum (Figs. 4 and 5) indicate a significant peak at 250–4400 cm^{-1} region due to the hydrogen saturation on metal surface by that clusters. IR of all cobalt clusters (shown in Fig. 4) show discrete band at 250–1500 cm^{-1} frequency region and frequency band shift to higher frequency with increasing number of captured hydrogen. Nickel clusters (shown in Fig. 5) show common band at around 1000 and 3500 cm^{-1} frequency region. IR spectrums also demonstrate the effect of hydrogen capturing on reduced cobalt surface. A vibrational frequency study attribute that both metal clusters are stable and promising since all cluster are free from imaginary frequency (Fig. 4 and Fig. 5). Four hydrogen molecules can be captured on reduced oxide surface with minimum energy on potential energy surface. The DFT calculation on reduced cobalt and nickel oxides predict the hydrogen adsorption capacity of 9 -13 wt% with minimum potential energy surface (PES).

Table 3
Cluster stability descriptors.

Cluster	E (kcal/mol)	η (kcal/mol)	χ (kcal/mol)	ω (kcal/mol)
Ni-(H_2)	-9.46×10^5	134.85	72.37	22.81
Ni-$(H_2)_2$	-9.47×10^5	145.91	79.99	21.90
Ni-$(H_2)_3$	-9.48×10^5	195.23	81.82	17.05
Ni-$(H_2)_4$	-9.49×10^5	205.15	83.45	16.83
Co-(H_2)	-8.67×10^5	187.16	267.61	149.36
Co-$(H_2)_2$	-8.68×10^5	264.16	263.23	131.15
Co-$(H_2)_3$	-8.69×10^5	269.91	254.01	119.39
Co-$(H_2)_4$	-8.70×10^5	273.38	246.63	111.11

Note: Total energy (E), hardness(η), electronegativity (χ), electrophilicity (ω).

4. Conclusions

The Hydrogen adsorption study using the density functional theory (DFT) via few quantum molecular (QM) reactivity descriptors

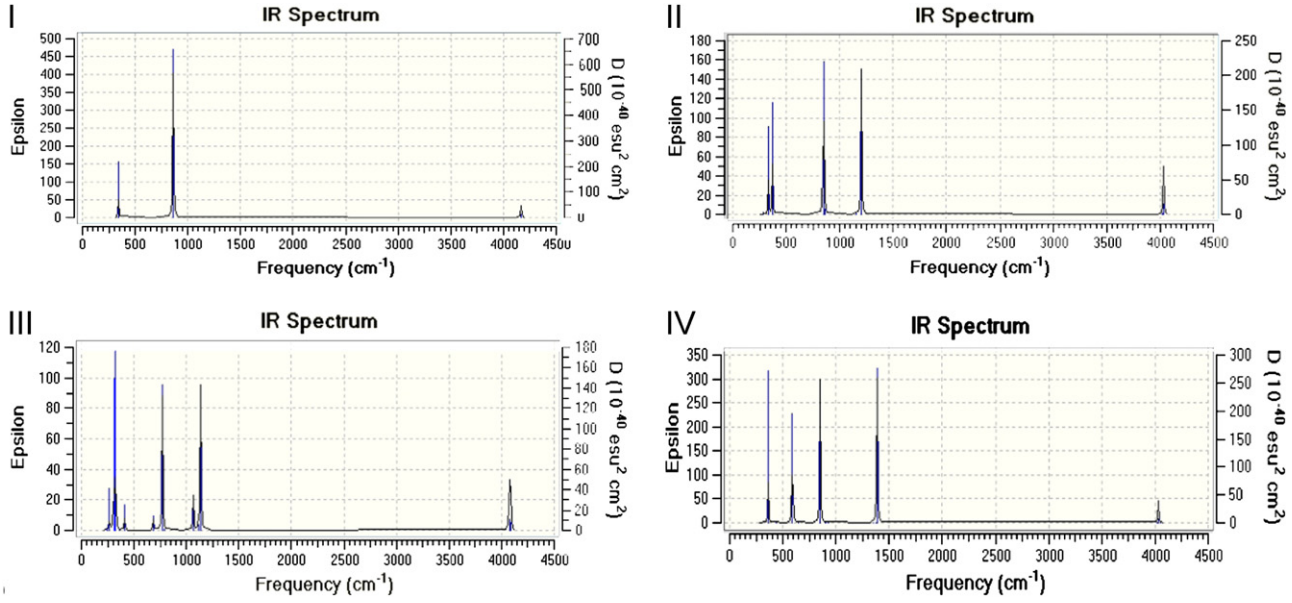

Fig. 4. Gaussian 09W software generated IR spectrum of Cobalt clusters: (I) Co-(H_2) (II) Co-$(H_2)_2$ (III) Co-$(H_2)_3$ (IV) Co-$(H_2)_4$.

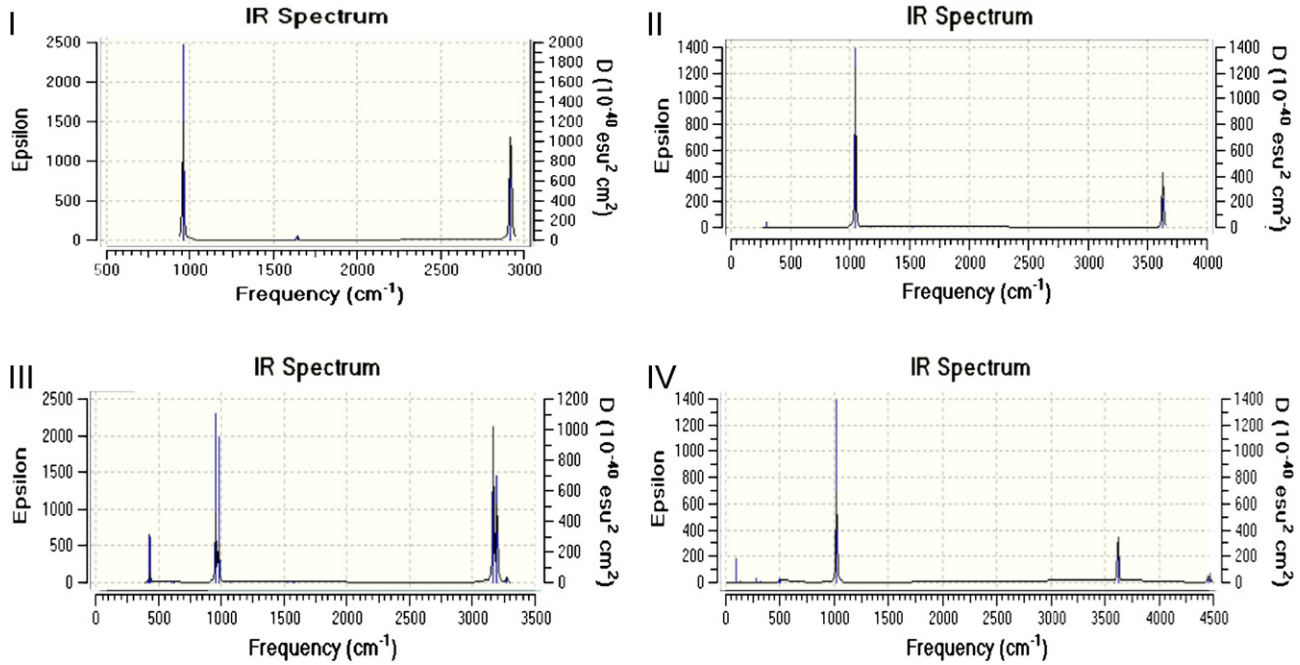

Fig. 5. Gaussian 09W software generated IR spectrum of nickel clusters: (I) Ni-(H_2) (II) Ni-(H_2)$_2$ (IV) Ni-(H_2)$_3$ (V) Ni-(H_2)$_4$.

has provided information on the adsorption feasibility and its successful application to find new hydrogen storage materials. Variation of the different reactivity descriptor values upon the increasing of captured hydrogen molecules implies the stability of the clusters and their feasibility. Computational results are consistent with experimental adsorption results that have been discussed through different reactivity descriptors. Both investigation methods confirm that the reduced mixed oxides are the promising candidate for hydrogen storage. Good interaction energy per hydrogen molecule and high hydrogen capacities are another advantage for selecting the promising hydrogen storage cluster.

Acknowledgements

We would like to acknowledge gratefully the financial support of this research by the FRGS grant 158-200-092, Malaysia and would like to thanks to department of Chemistry, University of Malaya, Malaysia for Computational support (Software).

Referances

[1] H. Nakatsuji, M. Hada, H. Ogawa, K. Nagata, K. Domen, J. Phys. Chem. 98 (1994) 11840.
[2] A. Gil, R. Trujillano, M.A. Vicente, S.A. Korili, Int. J. Hydrogen Energy 34 (2009) 8611.
[3] A. Hofmann, S.J. Clark, M. Oppel, I. Hahndorf, Phys. Chem. Chem. Phys. 4 (2002) 3500.
[4] C.W. Hu, Y.Q. Chen, P. Li, H. Min, Y. Chen, A. Tian, J. Mol. Catal. A: Chem. 110 (1996) 163.
[5] L. Jalowiecki-Duhamela, J. Carpentiera, A. Ponchelb, Int. J. Hydrogen Energy 32 (2007) 2439–2444.
[6] F. Greuter, I. Strathy, E.W. Plummer, W. Eberhardt, Phys. Rev. B: Condens. Matter 33 (1986) 736.
[7] H.J. Robota, W. Vielhaber, M.C. Lin, J. Segner, G. Ertl, Surf. Sci. 155 (1985) 101.
[8] Z.Y. Zhong, Z.T. Xiong, L.F. Sun, J.Z. Luo, P. Chen, X. Wu, J. Lin, K.L. Tan, J. Phys. Chem. B 106 (2002) 9507–9513.
[9] C.H. Bartholomew, Catal. Lett. 7 (1990) 27.
[10] R. Lochan, M. Head-Gordon, Phys. Chem. Chem. Phys. 8 (2006) 1357–1370.
[11] H. Smithson, C.A. Marianetti, D. Morgan, A. Van der Ven, A. Predith,1, G. Ceder, Phys. Rev. B: Condens. Matter 66 (2002) 144107.
[12] A. Emilbus, Uribe, C. Mar tha, D. José, L. Villaveces, Chem. Phys. Lett. 4 (90) (2010) 143–147.
[13] W. An, X. Wu, X.C. Zeng, J. Phys. Chem. C 112 (2008) 5747.
[14] X.T. Shu, H.L. Peter, A. Notten, Rutger, V. Santen, P.J. Antonius, J. Alloys Compd. 509 (2011) 210–216.
[15] (a) S. Chaudhuri, J. Graetz, A. Ignatov, J.J. Reilly, J.T. Muck erman, J. Am. Chem. Soc. 128 (35) (2006) 11404–11415;
(b) I. Ljubic, D.C. Clary, Phys. Chem. Chem. Phys. 12 (2010) 4012.
[16] J.L.C. Rowsell, O.M. Yaghi, Angew. Chem. Int. Ed. 44 (2005) 4670–4679.
[17] J.L.C. Roswell, O.M. Yaghi, J. Am. Chem. Soc. 128 (2006) 1304–1315.
[18] K. Sillar, A. Hofmann, J. Sauer, J. Am. Chem. Soc. 131 (2009) 4143–4150.
[19] (a) A.C. Dillon, K.M. Jones, T.A. Bekkedahl, C.H. Kiang, D.S. Bethune, M.J. Heben, Nature 38612 (1997) 377–379;
(b) G.E. Froudakis, Phys. Rev. B: Condens. Matter 14 (2002) R453;
(c) S.N. Yurchenko, J. Breidung, W. Thiel, Theor. Chem. Acc. 144 (2005) 333–340.
[20] (a) A. Züttel, P. Sudan, Ph. Mauron, T. Kiyobaiashi, Ch. Emmenegger, L. Schlapbach, Int. J. Hydrogen Energy 27 (2002) 203–212;
(b) J.B. Martin, I.A. Kinloch, R.A.W. Dryfe, J. Phys. Chem. C 114 (10) (2010) 4693–4703;
(c) A. Du, Z. Zhu, S.C. Smith, J. Am. Chem. Soc. 132 (2010) 2876.
[21] (a) T.A. Strobel, Y. Kim, G.S. Andrews, J.R. Ferrell III, C.A. Koh, A.M. Herring, E.D. Sloan, J. Am. Chem. Soc. 130 (2008) 14975;
(b) F. Su, C.L. Bray, B. Tan, A.I. Cooper, Adv. Mater. 20 (2008) 2663.
[22] Y. Liang, H.B. Dai, L.P. Ma, P. Wang, H.M. Cheng, Int. J. Hydrogen Energy 35 (2010) 3023–3028.
[23] P.W. Ayers, R.G. Parr, J. Am. Chem. Soc. 2000 (2010) 122.
[24] P. Fuentealba, Y. Simon-Manso, P.K. Chattaraj, J. Phys. Chem. A 104 (2000) 3185.
[25] R. Parthasarathi, M. Elango, V. Subramanian, P.K. Chattaraj, Theo. Chem. Acc. 113 (2005) 257.
[26] S. Pan, S. Giri, P.K. Chattaraj, J. Comput. Chem. 33 (4) (2012) 425–434.
[27] Y. Lwin, M.A. Yarmo, Z. Yaakob, A.B. Mohamad, W.A.W. Daud, Mater. Res. Bull. 36 (2001) 193–198.
[28] Y. Zhao, N.E. Schultz, D.G. Truhlar, J. Chem. Theory Comput. 2 (2006) 364–382.
[29] W.J. Hehre, L. Radom, P.V.R. Schleyer, J.A. Pople, Ab Initio Molecular Orbital Theory, JohnWiley & Sons, New York, 1987.
[30] M.J. Frisch, G.W. Trucks, H.B. Schlegel, G.E. Scuceria, M.A. Robb, J.R. Cheeseman, G. Scalmani, V. Barone, B. Mennucci, G.A. Petersson, H. Nakatsui, M. Caricato, X. Li, H.P. Hratchian, A.F. Izmaylov, J. Bloino, G. Zheng, J.L. Sonnenberg, M. Hada, M. Ehara, K. Toyota, R. Fukuda, J. Hasegawa, M. Ishida, T. Nakajima, Y. Honda, O. Kitao, H. Nakai, T. Vreven, J.A. Montgomery Jr., J.E. Peralta, F. Ogliaro, M. Bearpark, J.J. Heyd, E. Brothers, K.N. Kudin, V.N. Stariverov, R. Kobayashi, J. Normand, K. Raghavachari, A. Rendell, J.C. Burant, S.S. Iyengar, J. Tomasi, M. Cossi, N. Rega, N.J. Millam, M. Klene, J.E. Knox, J.B. Cross, V. Bakken, C. Adamo, J. Jaramillo, R. Gomperts, R.E. Stratmann, O. Yazev, A.J. Austin, R. Cammi, C. Pomelli, J.W. Ochterski, R.I. Martin, K. Morokuma, V.G. Zakrzewski, G.A. Voth, P. Salvador, J.J. Dannenberg, S. Dapprich, A.D. Daniels, O. Farkas, J.B. Foresman, J.V. Ortiz, J. Cioslowski, D.J. Fox, Gaussian 09, Revision A.1, Gaussian Inc., Wallingford C.T., 2009.
[31] (a) K.D. Sen, C.K. Jorgenson (Eds.), Electronegativity, vol. 66, Springer, Berlin, 1987;

(b) R.G. Parr, R.A. Donnelly, M. Levy, W.E. Palke, J. Chem. Phys. 68 (1978) 3801–3807.
[32] (a) R.G. Parr, R.G. Pearson, J. Am. Chem. Soc. 105 (1983) 7512–7516;
(b) K.D. Sen, D.M.P. Mingos (Eds.), Chemical Hardness, vol. 80, Springer, Berlin, 1993;
(c) R.G. Pearson, Chemical Hardness:Applications from Molecules to Solids, Wiley-VCH, Weinheim, 1997.
[33] (a) R.G. Parr, L.V. Szentpaly, S. Liu, J. Am. Chem. Soc. 121 (1999) 1922;
(b) P.K. Chattaraj, D.R. Roy, Chem. Rev. 107 (2007) PR46–PR74.
[34] T.J.D. Kumar, P. Tarakeshwar, N. Balakrishnan, Phys. Rev. B 79 (2009) 205415.
[35] J. Ochterski, Thermochemistry in Gaussian, Gaussian, Inc., 2000.
[36] Z. Ping, J. Zhang, M.O. Adebajo, H. Zhang, C. Zhou, Appl. Clay Sci. 53 (2) (2011) 139–150.
[37] J.G. Kim, D.L. Pugmire, D. Battaglia, M.A. Langell, Appl. Surf. Sci. 165 (1) (2000) 70–84.
[38] S. Ribet, D. Tichit, B. Coq, B. Ducourant, F. Morato, J. Solid State Chem. 142 (1999) 382.
[39] A.H. Natanael, A.L. Marla, W.P. Oscar, Catal. Lett. 141 (2011) 1018.
[40] S.J. Kerber, J.J. Bruckner, K. Wozniak, S. Seal, S. Hardcastle, S.T. Barr, J. Vac. Sci. Technol., A 14 (3) (1996) 234–239.
[41] M.G. Nijkamp, J.E.M.J. Raaymakers, A.J. van Dillen, K.P. de Jong, Appl. Phys. A 72 (2001) 619–623.
[42] I. Swart, A. Fielicke, B. Redlich, G. Meijer, B.M. Weckhuysen, F.M.F. d Groot, J. Am. Chem.Soc. 192 (2007) 2516–2520.
[43] I. Wart, F.M.F.d. Groot, B.M. Weckhuysen, P. Gruene, G. Meijer, A. Fielicke, Phys. Chem. A 112 (6) (2008) 1139–1149.